Applied Catalysis B: Environment and Energy 344 (2024) 123640

Contents lists available at ScienceDirect

Applied Catalysis B: Environment and Energy

journal homepage: www.elsevier.com/locate/apcatb

Novel durable and recyclable Cu@MoS_2/polyacrylamide/copper alginate hydrogel photo-Fenton-like catalyst with enhanced and self-regenerable adsorption and degradation of high concentration tetracycline

Gang Qin [a,b,1], Xiaoyu Song [a,b,1], Qiang Chen [d], Wenjie He [a], Jia Yang [a], Yue Li [b,*], Yongcai Zhang [c,*], Jun Wang [e,*], Dionysios D. Dionysiou [f]

[a] School of Materials Science and Engineering, Henan Polytechnic University, Jiaozuo 454003, China
[b] School of Chemical and Printing-Dyeing Engineering, Henan International Joint Laboratory of Rare Earth Composite Materials, Henan University of Engineering, Zhengzhou 451191, China
[c] School of Chemistry and Chemical Engineering, Yangzhou University, Yangzhou 225009, China
[d] Wenzhou Institute, University of Chinese Academy of Sciences, Wenzhou 352001, China
[e] College of Physics, Chongqing University, Chongqing 401331, China
[f] Environmental Engineering and Science Program, Department of Chemical and Environmental Engineering, University of Cincinnati, Cincinnati, OH 45221, USA

ARTICLE INFO

Keywords:
Hydrogel
Photo-Fenton-like catalyst
Synergic effect
Adsorption
Degradation
Tetracycline

ABSTRACT

A durable and recyclable Cu@MoS_2/polyacrylamide/copper alginate nanocomposite double network (Cu@MoS_2/PAAm/CA NCDN) hydrogel photo-Fenton-like catalyst was prepared for efficient removal of high concentration tetracycline (TC) in pharmaceutical wastewater. This hydrogel catalyst exhibits a remarkable synergistic effect between adsorption and catalytic degradation of TC. Consequently, this hydrogel catalyst shows a larger TC adsorption capacity of 122.2 mg g^{-1} and a higher TC degradation efficiency of 90% (degradation amount = 70.2 mg g^{-1}) at the TC concentration of 200 mg L^{-1}, while the TC degradation efficiency by Cu@MoS_2 catalyst is only 19% (degradation amount = 38.2 mg g^{-1}). This hydrogel catalyst can effectively remove high concentration TC under both light and dark conditions. Moreover, the tensile strength of Cu@MoS_2/PAAm/CA NCDN hydrogel catalyst reaches an extraordinary 1.46 MPa and maintains 0.68 MPa after 15-day immersion in water, indicating high durability. In addition, the flexible hydrogel catalyst can keep good integrity after being deformed by stretching, bending, and knotting, etc., enabling its easy recovery. This investigation provides an innovative and versatile strategy to develop high-performance hydrogel catalysts for treating antibiotics-polluted water.

1. Introduction

With the mass production and widespread use of antibiotics, the environmental risk of antibiotics has aroused great concern worldwide [1–3]. Antibiotics usually show high resistance to natural degradation and can lead to the development of microorganisms that are resistant to antibiotics, thereby posing a threat to ecosystem and human health. Tetracycline (TC) antibiotics are currently the second most commonly used antibiotics across the world. As a result, TC is among the most often detected antibiotics in the waters of many places in China, and its concentration is ever-increasing. Particularly, high concentration residue of TC in pharmaceutical wastewater (> 100 mg L^{-1}) has been frequently detected due to its production process and technical reasons [4–6]. However, high concentration TC has a strong inhibition and killing effect on microorganisms in wastewater biochemical treatment. Hence, it is very urgent to develop other promising approaches to eliminate high concentration TC from water.

Adsorption is a highly efficient technology for removing antibiotic pollutants from water. So far, many different types of adsorbents have been developed [7–11]. Most previous studies have focused on improving the adsorption capacity of adsorbents, but the treatment of the adsorbed pollutants, the regeneration of the adsorbents, and the continuous renewal of the adsorption during the degradation process are often neglected [12].

* Corresponding authors.
E-mail addresses: liyue0128@163.com (Y. Li), zhangyc@yzu.edu.cn (Y. Zhang), junwang2021@cqu.edu.cn (J. Wang).
[1] These authors contributed equally to this work.

https://doi.org/10.1016/j.apcatb.2023.123640
Received 20 August 2023; Received in revised form 27 November 2023; Accepted 16 December 2023
Available online 20 December 2023

Advanced oxidation processes are promising methods to eliminate antibiotic pollutants in water. As one of the advanced oxidation technologies, the photo-Fenton-like reaction is widely utilized to degrade antibiotic pollutants, because the photo-induced electrons can rapidly transfer and generate active radicals [13–15]. In addition, compared with the traditional Fe^{2+}/Fe^{3+} system, Cu^{+}/Cu^{2+} system can faster react with H_2O_2 to generate hydroxyl radicals (·OH), making it more suitable for oxidative degradation of organic pollutants [16,17]. However, most studies of Fenton-like catalysts focus only on the catalytic degradation reactions [18]. The synergistic effect between catalytic degradation and adsorption of high concentration antibiotics is ignored, limiting the removal capacities of the Fenton-like catalysts. For instance, some references report adsorption capacities of merely 3, 10, 3, and 1 mg g^{-1}, while catalytic degradation amounts of only 25, 15, 30, and 9 mg g^{-1} [19–22]. Therefore, the mutual promotion between the adsorption and catalytic degradation performance of Fenton-like catalysts is worthy of in-depth study to improve the pollutant removal rate and efficiency of catalysts.

MoS_2 is a two-dimensional (2D) transition metal sulfide semiconductor with active edge sites [23,24]. It has the potential to act as a highly effective Fenton-like catalyst, because it can catalyze the decomposition of H_2O_2 into·OH [25]. The Mo^{4+} is oxidized by H_2O_2 to generate •OH by Eq. 3. Meanwhile, Mo^{5+} and Mo^{6+} are reduced to Mo^{4+} via Eq. 4. Moreover, Mo^{4+} can also further react with variable-valence metal ions (Eq. 5), thus promoting a faster cycle of valence change and a more efficient generation of the active radicals. Hence, the introduction of MoS_2 will accelerate the conversion rate of the Cu^{+}/Cu^{2+} system, as depicted in Eqs. (1−7) [16,26].

$$Cu^{+} + H_2O_2 \rightarrow Cu^{2+} + HO\cdot + HO^{-} \ (k = 1{\cdot}0\times10^{4}\ L{\cdot}mol^{-1}{\cdot}s^{-1}) \quad (1)$$

$$Cu^{2+} + H_2O_2 \rightarrow Cu^{+} + \cdot O_2H + H^{+} \ (k = 4{\cdot}6\times10^{2}\ L{\cdot}mol^{-1}{\cdot}s^{-1}) \quad (2)$$

$$Mo^{4+} + H_2O_2 \rightarrow Mo^{5+}/Mo^{6+} + OH^{-} + \cdot OH \quad (3)$$

$$Mo^{6+}/Mo^{5+} + H_2O_2 \rightarrow Mo^{4+} + \cdot O_2H + H^{+} \quad (4)$$

$$Mo^{4+} + 2Cu^{2+} \rightarrow Mo^{6+} + 2Cu^{+} \quad (5)$$

$$Mo^{6+} + H_2O_2 \rightarrow Mo^{4+} + 2\,H^{+} + O_2 \quad (6)$$

$$Cu^{+} + O_2 \rightarrow O_2^{\bullet-} + Cu^{2+} \quad (7)$$

However, traditional Fenton-like catalysts are mostly in powder form, making them difficult to be recycled due to their tiny structure. To address this issue, a prospective strategy is to immobilize nano-catalysts on low-cost 3D support materials to improve utilization efficiency and reduce recycling costs. Hydrogels are widely utilized in various fields due to their 3D porous structure, large surface area, excellent hydrophilicity and adsorption properties [27,28]. However, it should be noted that the application of hydrogels in wastewater treatment relies only on adsorption, which cannot indeed degrade organic pollutants and achieve self-regeneration [29–31]. Furthermore, most reported hydrogels are limited by their poor mechanical properties [32]. At present, nanocomposite double network (NCDN) hydrogels have drawn increasing attention because of their high strength and ductility [33,34]. The first network of NCDN hydrogels comprises a densely crosslinking rigid and brittle polymer in combination with nanoparticles; while their second network is formed by a soft but malleable polymer [35]. The synergy between double networks and nanoparticles gives the hydrogel excellent mechanical properties [36,37]. Therefore, the NCDN hydrogels are considered to have great application potential in treating wastewater contaminated with antibiotics and other contaminants of emerging concern.

Considering all the above factors, we developed a novel durable and recyclable Cu@MoS_2/PAAm/CA NCDN hydrogel catalyst with outstanding performance in both adsorption and catalytic degradation of high concentration TC. The double network hydrogel, which consists of the first network of CA crosslinked by Cu^{2+} and the second network of PAAm via in-situ polymerization, acts as the catalyst support. Meanwhile, Cu@MoS_2 plays a dual role: a Fenton-like catalyst, and a multi-arm crosslinking agent which can react with the CA network. The Cu@MoS_2/PAAm/CA NCDN hydrogel catalyst has the following outstanding features: (i) significantly enhanced mechanical properties due to the interaction of its double network structure and MoS_2 nanosheets; (ii) superior performance in both adsorption and catalytic degradation of high concentration TC. The synergistic effect between adsorption and catalytic degradation can achieve mutual promotion. The adsorption process can enrich TC around the catalyst, which is beneficial to reduce the travel distance of the reactive species and accelerate the reaction rate. On the other hand, the catalytic degradation process eliminates TC and regenerates the adsorption sites, endowing the hydrogel catalyst with renewable adsorption ability; (iii) easy recycling because the 3D network structure of the hydrogel can firmly immobilize the catalytically active Cu@MoS_2; and (iv) long-term stability and durability for antibiotic wastewater treatment. Hence, it is expected that the innovative Cu@MoS_2/PAAm/CA NCDN hydrogel catalyst, with great synergistic effect between adsorption and catalytic degradation, remarkable recyclability, excellent mechanical performance, and outstanding durability, can offer a promising solution for treating high concentration antibiotic wastewater.

2. Experiment

2.1. Reagents

The main reagents used in our current work are listed in Supporting Information.

2.2. Preparation

2.2.1. Preparation of Cu@MoS_2

Cu@MoS_2 was prepared via the following two steps:

(1) Preparation of MoS_2 by hydrothermal method. In 35 mL of deionized water, 1 mmol L^{-1} $(NH_4)_6Mo_7O_{24}{\cdot}4\ H_2O$ and 15 mmol L^{-1} CH_4N_2S were dissolved at ambient temperature. The mixed solution was infused into a 50 mL polytetrafluoroethylene-lined high-pressure reaction kettle and heated at 210 °C for 24 h. When cooled to ambient temperature, the formed sample was centrifuged, and washed three times alternately with deionized water and anhydrous ethanol to remove impurities. Finally, the sample was placed in an oven and dried at 60 °C for 8 h.

(2) Preparation of Cu@MoS_2 by photo-deposition method. 1 g MoS_2 was soaked in 100 mL 0.5 mol L^{-1} $CuSO_4$ aqueous solution for 7 h, then irradiated using a xenon lamp under N_2 protection for 1 h.

2.2.2. Preparation of Cu@MoS_2/PAAm/CA NCDN hydrogel catalyst

The Cu@MoS_2/PAAm/CA NCDN hydrogel catalyst was synthesized via the following steps. Firstly, 0.5 g sodium alginate (SA) was dissolved in 10 mL deionized water and stirred continuously for 30 min at 65 °C. Then, 1.4 g acrylamide (AM), 0.1 g MoS_2, 48.8 μL N, N-methylenebisacrylamide (MBAA), and 0.047 g photo-initiator (2-hydroxy-4′-(2-hydroxyethoxy)− 2-methylpropiophenone) were dispersed in the SA solution and stirred slowly for 60 min. Next, the bubbles in the solution were removed by filling with N_2 for 10 min. The as-prepared gel precursor solution was injected into a mold (160 mm × 120 mm × 1 mm) and irradiated by UV light for 60 min to convert it to hydrogel. The obtained hydrogel was immersed in 0.5 mol L^{-1} $CuSO_4$ aqueous solution for 7 h, then irradiated with xenon lamp for 1 h. The irradiation process was under N_2 protection. After the irradiation process, the hydrogel was immersed 12 h with deionized water to eliminate loosely attached $CuSO_4$. Thus, a Cu@MoS_2/PAAm/CA NCDN hydrogel catalyst with excellent toughness was obtained. By using the same method, the control samples (PAAm/SA hydrogel, PAAm/CA hydrogel catalyst, MoS_2/PAAm/SA hydrogel catalyst and Cu@MoS_2/PAAm/CA NCDN hydrogel

catalyst with varying proportions) were also fabricated.

2.3. Characterization

The main characterization means used in this work are described in Supporting Information.

2.4. Mechanical testing

The hydrogel catalyst was cut into 1 mm thick dumbbell-shaped strips. The tensile test was done at a tensile rate of 100 mm min^{-1} on a universal testing machine (WSM-10KN, Changchun Intelligent Instrument Equipment Co., Ltd., China). Each experiment was repeated 3 times [38].

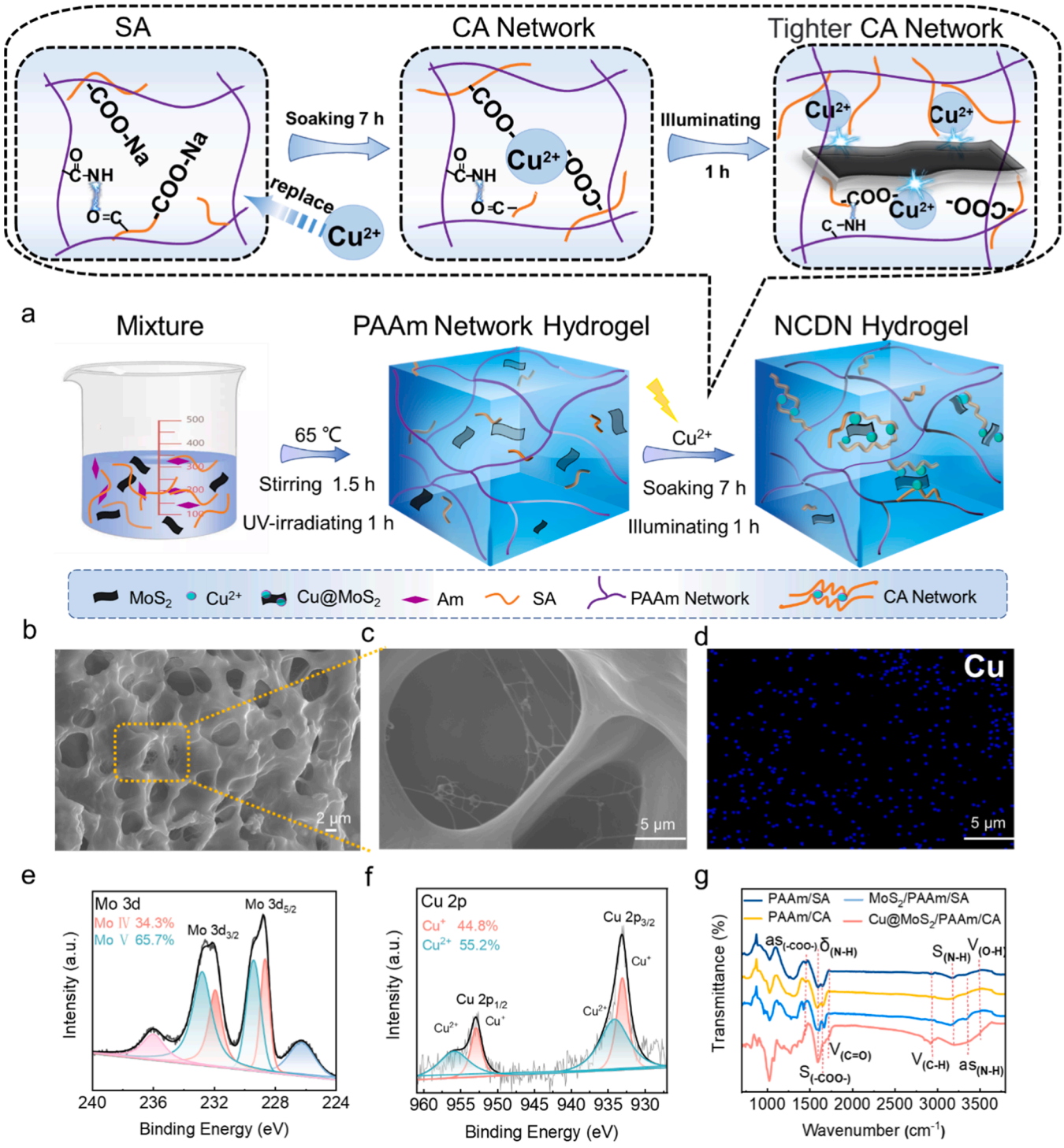

Fig. 1. (a) Synthesis processes of the Cu@MoS_2/PAAm/CA NCDN hydrogel catalyst; (b) SEM image of the Cu@MoS_2/PAAm/CA NCDN hydrogel catalyst; (c) partial enlargement of the SEM image of the Cu@MoS_2/PAAm/CA NCDN hydrogel catalyst; (d) SEM-EDS element mapping image of the Cu@MoS_2/PAAm/CA NCDN hydrogel catalyst; XPS spectra of the Cu@MoS_2/PAAm/CA hydrogel catalyst: (e) Mo 3d and (f) Cu 2p; (g) FTIR spectra of the PAAm/SA hydrogel, PAAm/CA hydrogel catalyst, MoS_2/PAAm/SA hydrogel catalyst, and Cu@MoS_2/PAAm/CA hydrogel catalyst.

2.5. Adsorption experiments

In a beaker containing 50 mg hydrogel catalyst and 50 mL TC (200 mg L^{-1}) solution, a series of dark adsorption experiments were implemented. To determine the concentration of TC in the solution in each experiment, the solution was scanned by spectrophotometer (TU-1901, Beijing Purkinje General Instrument Co, China) to monitor the change in absorbance at the maximum absorbance wavelength (355 nm). The TC adsorption capacity (q_e) of the hydrogel catalyst was calculated according to Eq. (S1).

2.6. TC degradation experiments

To test the catalytic activity of Cu@MoS_2/PAAm/CA NCDN hydrogel catalyst for the degradation of TC, a series of experiments were conducted under different conditions, such as different H_2O_2 concentration, different MoS_2 dosages, with or without light irradiation. Firstly, 50 mg Cu@MoS_2/PAAm/CA hydrogel catalyst was immersed in 50 mL of 200 mg L^{-1} TC solution. The mixture was stirred in the dark for 48 h for establishing the adsorption-desorption equilibrium. Subsequently, to initiate the photo-Fenton-like catalytic reactions, H_2O_2 was added (the resulting solution contained 1.5 mmol L^{-1} H_2O_2) and the mixture was exposed to a xenon lamp (300 W, 320–780 nm, PLS-SME 300E, Bejing PerfectLight Technology Co, Ltd., China). At time intervals of 30 min, 2 mL of reaction solution was taken out and its absorbance was measured by UV-Vis spectrophotometer to determine the TC concentration. The catalyst reusability testing experiments, active species trapping experiments, and other pollutant removal experiments were also carried out, and the experimental details are described in Supporting Information.

2.7. Mechanical stability performance

To measure its mechanical stability in the water environment, the Cu@MoS_2/PAAm/CA hydrogel catalyst was immersed in deionized water for 3, 6, 9, 12, and 15 days, and the mechanical properties were assessed by tensile strength and elongation at break. Every experiment was repeated three times in parallel.

3. Results and discussion

3.1. Structural and compositional characterization

The formation process of the Cu@MoS_2/PAAm/CA NCDN hydrogel catalyst is depicted in Fig. 1a. Firstly, the hydrophilic PAAm network (second network) was fabricated by free radical polymerization, while the SA chains penetrated into the PAAm network and formed hydrogen bonds with it. At the same time, the MoS_2 nanosheets uniformly dispersed into the 3D structure of the resulting PAAm/SA hydrogel. Secondly, the MoS_2/PAAm/SA hydrogel catalyst was immersed in a $CuSO_4$ solution for 7 h and then photo-deposited for 1 h to obtain Cu@MoS_2/PAAm/CA NCDN hydrogel catalyst. During immersion, the ionic crosslinking CA network (first network) was formed through the replacement reaction between Cu^{2+} ions and G blocks on SA chains via "egg box modal". Moreover, a Cu@MoS_2 composite was generated during photo-deposition. In addition to serving as a bimetallic Fenton-like catalyst, the Cu@MoS_2 composite also acted as a multi-arm crosslinking agent for the CA network to improve the crosslinking density. The synergy of the double network structure and Cu@MoS_2 nanosheets endows the hydrogel catalyst with excellent mechanical properties. Moreover, the hydrogel catalyst can be directly recycled due to its variable macroscopic 3D shape, which avoids the separation problem of powder catalysts and makes it highly promising for practical applications.

SEM was utilized to scrutinize the 3D structure and surface morphology of the as-prepared hydrogel catalyst. As observed in Fig. 1b-c, the hydrogel catalyst possesses a distinctive porous structure, which not only increases the specific surface area, but also offers numerous footholds for the Cu@MoS_2 catalyst. As can be seen from Tab. S1, the specific surface area of Cu@MoS_2/PAAm/CA hydrogel catalyst is up to 225.66 m^2 g^{-1}, which is 23.6 times that of MoS_2. Meanwhile, the abundant pores act as water transport channels, providing beneficial condition for the contact between catalyst and pollutants. Compared with the PAAm/SA hydrogel and PAAm/CA hydrogel catalyst (Fig. S1), the Cu@MoS_2/PAAm/CA NCDN hydrogel catalyst exhibits a denser and more uniform pore structure. The decrease in pore size is attributed to the increased crosslinking density, which facilitates the construction of a more robust hydrogel catalyst. Notably, a "woven mesh" structure is observed in the pores of the Cu@MoS_2/PAAm/CA hydrogel catalyst (Fig. 1c). This is due to the "multi-arm crosslinking" provided by Cu@MoS_2, which further promotes the crosslinking of the CA network. This multiple network structure endows the Cu@MoS_2/PAAm/CA NCDN hydrogel catalyst with excellent mechanical strength and toughness. In addition, it can be confirmed by the SEM-EDS spectra (Fig. 1d-f) that MoS_2 and Cu components disperse uniformly over the hydrogel. Thus, light can irradiate the bimetallic Fenton-like catalysts in all directions, benefiting the maximum utilization of incident light energy.

The chemical state of Cu@MoS_2/PAAm/CA NCDN hydrogel catalyst was studied by XPS. The survey spectrum in Fig. S2a reveals the coexistence of O, C, N, Mo, S and Cu in the hydrogel catalyst. The Mo 3d spectrum shows two peaks at 229.5 eV and 233.7 eV that are consistent with the $3d_{5/2}$ and $3d_{3/2}$ of Mo^{4+} (Fig. 1e). Besides, other two peaks at 228.7 eV and 232.1 eV are in agreement with $3d_{5/2}$ and $3d_{3/2}$ of Mo^{5+}. Two major peaks appear in the S 2p spectrum at 163.45 eV and 162.21 eV (Fig. S2b), which are in turn assigned to $2p_{1/2}$ and $2p_{3/2}$ of S^{2-}. In Fig. 1f, the peaks at 933.7 and 954.4 eV are corresponding to $2p_{3/2}$ and $2p_{1/2}$ of Cu^{2+}, while the peaks at 932.2 and 952.1 eV are in agreement with the $2p_{3/2}$ and $2p_{1/2}$ of Cu^{+}. In general, the XPS results further corroborate that Cu@MoS2/PAAm/CA NCDN hydrogel catalyst are successfully prepared [39]. In addition, the XPS analysis of pure MoS_2 and Cu@MoS_2 was also carried out, and the corresponding results are detailed in Supporting Information (Fig. S3 and S4).

The chemical compositions of the Cu@MoS_2/PAAm/CA NCDN hydrogel catalyst and control samples (PAAm/SA hydrogel, PAAm/CA hydrogel catalyst, and MoS_2/PAAm/SA hydrogel catalyst) were analyzed using FTIR. The characteristic peaks of PAAm can be observed in the FTIR spectra of all samples (Fig. 1g), including the symmetrical vibration (3176 cm^{-1}), antisymmetric vibration (3420 cm^{-1}), and deformation vibration (1601 cm^{-1}) of N-H, the stretching vibration (2931 cm^{-1}) of C-H, and stretching vibration (1735 cm^{-1}) of C═O, indicating the successful polymerization of AM [34,36]. In the FTIR spectra of PAAm/SA hydrogel and MoS_2/PAAm/SA hydrogel catalyst, the peak at 3478 cm^{-1} is assigned to the stretching vibration of O-H, while the peaks at 1650 cm^{-1} and 1452 cm^{-1} are generated by the symmetric and antisymmetric vibrations of -COO^- of the SA, respectively [34,40]. For the PAAm/CA hydrogel catalyst, Cu^{2+} forms coordination bonds with -COO^- on the SA segment, as evidenced by the blue-shift of symmetric vibration (-COO^-) and the red-shift of antisymmetric vibration (-COO^-) [38,41]. The similar but more significant shifts of -COO^- can be observed in the FTIR spectrum of Cu@MoS_2/PAAm/CA hydrogel catalyst, also revealing the generation of coordination bonds between Cu^{2+} and -COO^- on SA [32]. In addition, the shift of C═O and N-H peaks is ascribed to the hydrogen bond formation between SA and PAAm [42]. These results confirm the successful formation of the CA network (first network) in the hydrogel catalyst.

Because hydrogels cannot be characterized by XRD and UV-Vis DRS, only the phase and light absorption property of Cu@MoS_2 were analyzed using XRD (Fig. S5) and UV-Vis DRS (Fig. S6). The XRD and XPS analysis results confirm that the Cu@MoS_2 nanosheets were successfully prepared by the photodeposition method (the detailed analysis is provided in the Supporting Information). The UV-Vis DRS analysis results in Fig. S6 demonstrate that the combination of Cu^{+}/Cu^{2+} and

MoS_2 can markedly improve the light absorption ability, thus contributing to more efficient utilization of solar energy.

3.2. Mechanical properties

Good mechanical properties of a hydrogel are crucial to its practical applications in wastewater treatment. Therefore, tensile experiments were conducted to investigate the mechanical properties of the Cu@MoS_2/PAAm/CA NCDN hydrogel catalyst. As shown in Fig. 2a, the covalent crosslinking PAAm/SA hydrogel is fragile, with a tensile strength of only 21 kPa and an elongation at break of 681%. However, the mechanical properties of the PAAm/SA hydrogel are further weakened by the addition of MoS_2, because the MoS_2 fillers disrupt the regularity of the crosslinking network (Fig. 2b I), resulting in stress defects [37]. This demonstrates that the MoS_2 nanosheets alone cannot interact with polymer chains to enhance the mechanical properties of the hydrogel. In contrast, after soaking in $CuSO_4$ solution, the ionic crosslinking CA network can be formed through the coordination between Cu^{2+} ions and the -COO^- on the SA chains (Fig. 2b II) [38]. The CA network interpenetrates with the PAAm network to form a PAAm/CA double network hydrogel catalyst, which has a tensile strength of 1.1 MPa (21 times higher than that of the PAAm/SA hydrogel). The high mechanical properties of the PAAm/CA hydrogel catalyst stem from the synergy between reversible ionic coordination and robust covalent crosslinking.

It is noteworthy that the tensile strength of the Cu@MoS_2/PAAm/CA NCDN hydrogel catalyst reaches an amazing 1.46 MPa, which is 28 times higher than that of the PAAm/SA hydrogel. The exceptional mechanical property of the Cu@MoS_2/PAAm/CA NCDN hydrogel catalyst can be attributed to the synergy between the Cu@MoS_2 nanocomposite and double network structure. Firstly, the CA network (the first network) intersperses into the PAAm network (the second network) backbone, improving the overall network density due to the entanglement between them via hydrogen bonds (Fig. 2b III) [38,42]. Secondly, the CA network shields the PAAm network from part of stresses, thus delaying rupture. Meanwhile, the deformable PAAm network is able to bridge the micro-fractures in the first CA network, ensuring the structure stability. Finally, the interaction between the Cu@MoS_2 multi-arm crosslinking agent and the CA network provides a higher crosslinking density of the CA network (Fig. 2b IV) [36]. Consequently, the imposed load will be efficiently distributed, reducing crack tip stress, and slowing crack propagation. In summary, the NCDN structure plays a vital role in stress transfer and energy dissipation, providing the Cu@MoS_2/PAAm/CA NCDN hydrogel catalyst with excellent mechanical properties and toughness. Besides, the influences of the dosages of AM, SA and MoS_2 on the tensile properties of the Cu@MoS_2/PAAm/CA NCDN hydrogel catalyst were examined, and the results obtained are presented in Fig. S7-9.

Swelling ratio is an important property of hydrogels, directly affecting their liquid diffusion ability [30,43]. The swelling ratio of the Cu@MoS_2/PAAm/CA NCDN hydrogel catalyst is shown in Fig S10, which exhibits an equilibrium expansion of 600%. Such an exceptional swelling ratio improves the efficiency of the mass transfer channel, making it easier for TC molecules to interact with the functional groups on the Cu@MoS_2/PAAm/CA NCDN hydrogel catalyst.

As shown in Fig. 2c-f, the Cu@MoS_2/PAAm/CA NCDN hydrogel catalyst can be easily stretched to approximately 4 times as its initial length in normal, crossed, knotted, and twisted stretching deformations.

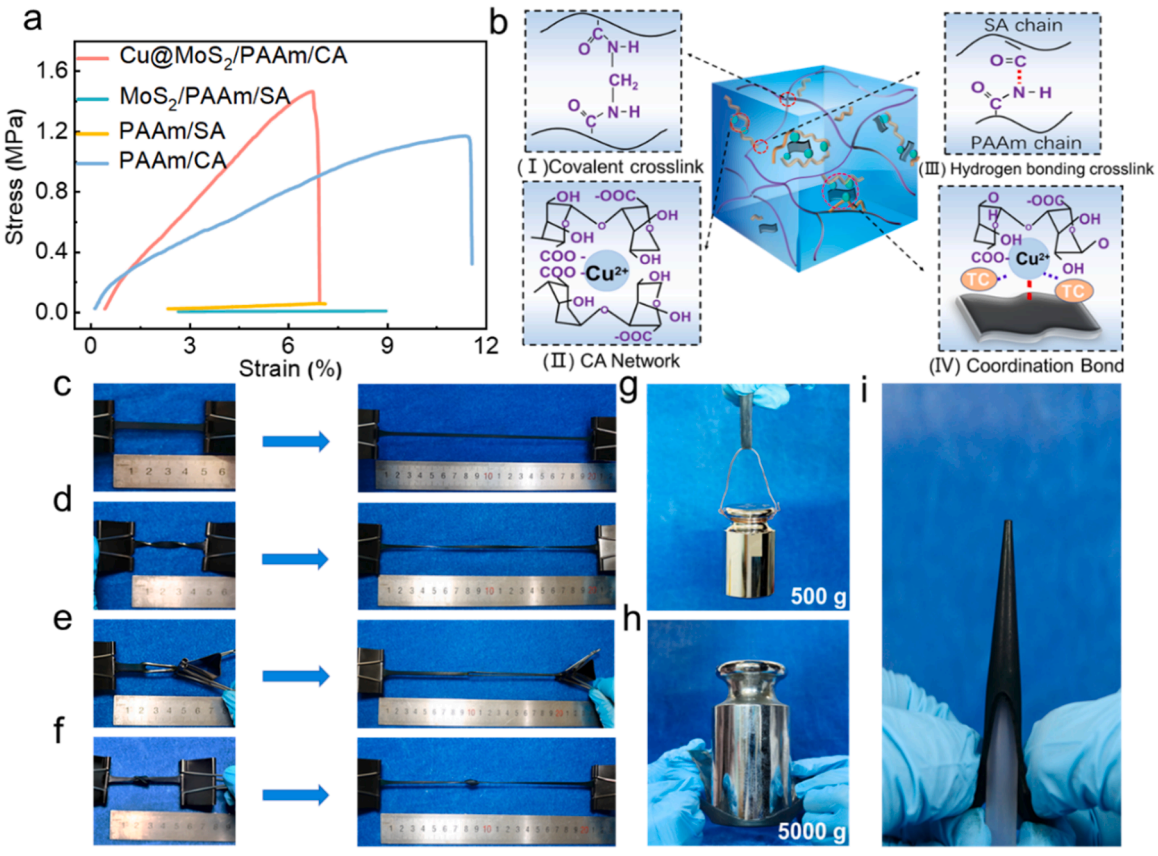

Fig. 2. (a) Tensile stress-strain curves of the PAAm/SA hydrogel, PAAm/CA hydrogel catalyst, MoS_2/PAAm/SA hydrogel catalyst, and Cu@MoS_2/PAAm/CA NCDN hydrogel catalyst; (b) schematic illustration of the molecular structure and proposed crosslinking mechanism of the hydrogel catalysts. The pictures demonstrating the mechanical performance of the Cu@MoS_2/PAAm/CA NCDN hydrogel catalysts: (c) stretching, (d) twisted stretching, (e) crossed stretching, (f) knotted stretching, (g) lifting a 500 g weight, (h) load-bearing, (i) puncturing.

Furthermore, it can also withstand hanging and pressure weights of 500 g and 5000 g, respectively (Fig. 2g and h). Additionally, as displayed in Fig. 2i, this hydrogel catalyst exhibits notable puncture resistance.

3.3. Adsorption of TC

In order to meet practical requirements, the design of the hydrogel catalysts with synergistic high-capacity adsorption and rapid degradation performance is urgently desired for wastewater treatment. The excellent hydrophilicity and adsorption performance enable the hydrogel catalyst to rapidly enrich TC from the solution (Fig. S11. water contact angle measurement). This is a prior step for full contact between the pollutant molecules and the active sites of catalyst, thereby facilitating rapid degradation during the following photo-Fenton-like catalysis process. However, the adsorption capacities of traditional catalysts are limited [21]. To determine their adsorption capacities for TC, the adsorption properties of Cu@MoS_2 nanosheets, PAAm/SA hydrogel, PAAm/CA hydrogel catalyst, MoS_2/PAAm/SA hydrogel catalyst, and Cu@MoS_2/PAAm/CA NCDN hydrogel catalyst were tested. As presented in Fig. 3a, the Cu@MoS_2 nanosheets (1.5 mg g^{-1}), PAAm/SA hydrogel (7.1 mg g^{-1}), and MoS_2/PAAm/SA hydrogel catalyst (9.7 mg g^{-1}) have only small capacities for TC adsorption. In contrast, the TC adsorption capacities of the PAAm/CA hydrogel catalyst and Cu@MoS_2/PAAm/CA NCDN hydrogel catalyst can reach 124.1 and 126.8 mg g^{-1}, respectively. Obviously, Cu^+/Cu^{2+} play a crucial role in increasing the TC adsorption on the Cu@MoS_2/PAAm/CA NCDN hydrogel catalyst. Furthermore, the Cu@MoS_2/PAAm/CA NCDN hydrogel catalyst has also higher adsorption capacity, compared with many recently reported counterparts (Tab. S2).

As shown in Fig. 3b, the TC adsorption capacity of the Cu@MoS_2/PAAm/CA NCDN hydrogel catalyst increases with the increase in SA concentration, indicating that SA and Cu^{2+} can directly affect the adsorption capacity. The -COONa groups on the SA chain react with Cu^{2+} to form $(-COO)_2Cu$ during immersion in $CuSO_4$ solution. Then, $(-COO)_2Cu$ can act as a "bridge" in the TC adsorption because of the Hard-Soft-Acid-Base theory and the spatial effect [44]. Therefore, the Cu@MoS_2/PAAm/CA NCDN hydrogel catalyst possesses excellent adsorption performance, endowing itself with the ability to contact pollutants quickly and realizing the synergistic effect between adsorption and catalytic degradation. However, the SA content in the hydrogel catalyst is limited by its solubility, restricting the maximum adsorption capacity. In addition, the TC adsorption performance of the Cu@MoS_2/PAAm/CA NCDN hydrogel catalyst prepared with different MoS_2 dosages was further researched (Fig. S12). The overall TC adsorption capacity of the Cu@MoS_2/PAAm/CA NCDN hydrogel catalyst remains almost unchanged with increasing the MoS_2 dosage, but the time required to reach adsorption equilibrium increases.

Initial pH influences not only the protonation of functional groups of the Cu@MoS_2/PAAm/CA NCDN hydrogel catalyst, but also the chemical properties and existing forms of TC in the solution [28,45]. The zeta potentials of the Cu@MoS_2/PAAm/CA NCDN hydrogel catalyst and speciation distributions of TC are shown in Fig. S13. Fig. 3c illustrates the effect of pH on the TC adsorption by the Cu@MoS_2/PAAm/CA NCDN hydrogel catalyst. At pH < 7, the TC molecule is considered a zwitterion with both positive and negative charge groups. At this time, three ion species, including TC^+, $TC^{\pm}$ and TC^-, are present simultaneously in the TC solution. At pH < 5, the zeta potential of the hydrogel catalyst is positive, and the main TC colony is TC^+. High concentration TC^+ inhibits TC adsorption on the hydrogel catalyst due to electrostatic repulsion. As pH increases, the relative ratio of TC^- increases and the zeta potential of the hydrogel catalyst decreases [45,46]. The electrostatic adsorption effect and ion exchange reach their peaks at pH = 5, resulting in a maximal adsorption capacity of 127.8 mg g^{-1}. At 5 < pH < 7, the relative ratio of TC^- further increases, and the zeta potential of the hydrogel catalyst becomes negative. Thus, the repulsive force between TC and the hydrogel catalyst intensifies, leading to a decrease in adsorption. However, variation of the pH only marginally impacts the TC adsorption capacity of the Cu@MoS_2/PAAm/CA NCDN hydrogel catalyst, providing a strong basis for its application in complex

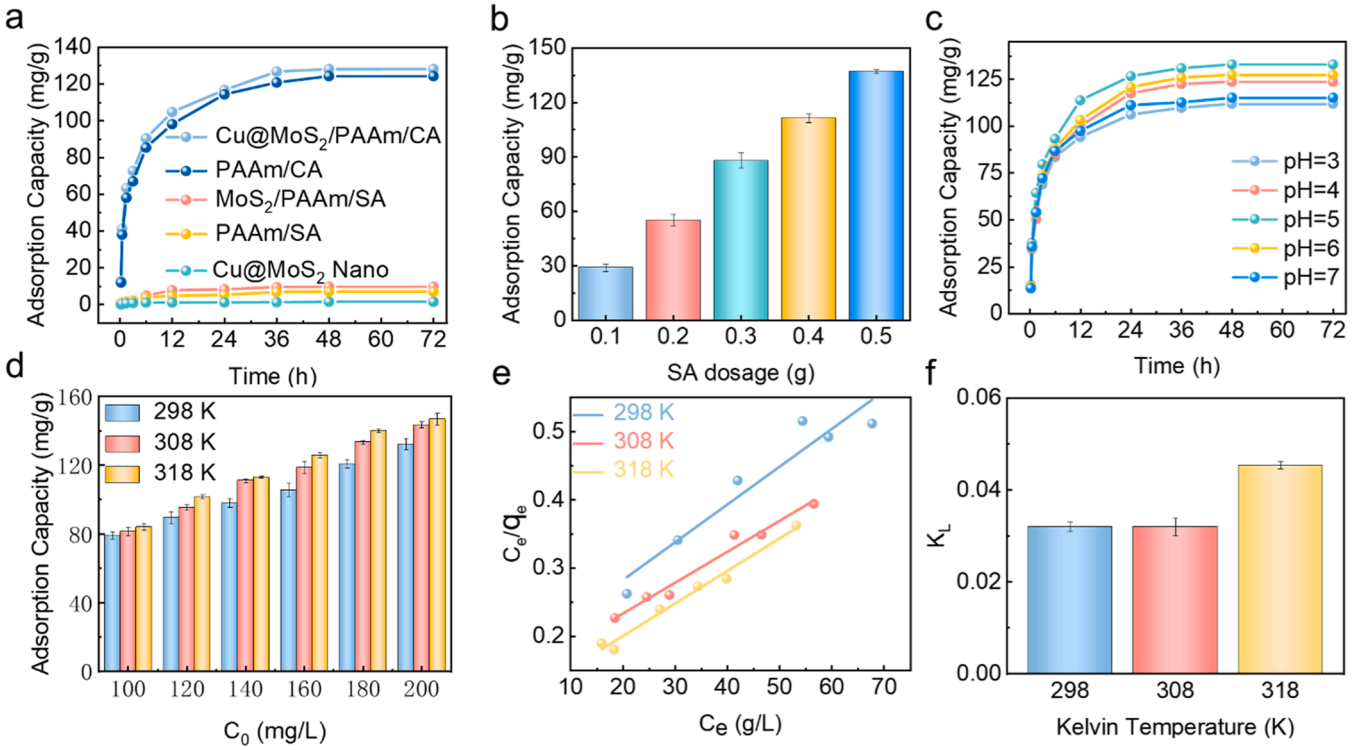

Fig. 3. Impacts of (a) composition of hydrogel, (b) dosage of SA, (c) initial pH value, (d) temperature and initial TC concentration on the TC adsorption by the Cu@MoS_2/PAAm/CA NCDN hydrogel catalyst. (e) Fitting plots of Langmuir model; (f) kinetic constants (K_L) obtained according to Langmuir model.

environments.

Besides, according to the influences of temperature and initial TC concentration, the adsorption isotherms and the three kinetic models were utilized to explore the adsorption mechanism of the Cu@MoS_2/PAAm/CA NCDN hydrogel catalyst [47–49]. As shown in Fig. 3d, with the increase of temperature (from 298 K to 318 K) and initial TC concentration (from 100 mg L^{-1} to 200 mg L^{-1}), the TC adsorption capacity of the Cu@MoS_2/PAAm/CA NCDN hydrogel catalyst also increases. However, the TC adsorption capacity of the Cu@MoS_2/PAAm/CA NCDN hydrogel catalyst increases only slightly when the TC concentration further increases from 200 to 240 mg L^{-1} at 298 K (Fig. S14). From Fig. 3e-f, Fig. S15 and Tab. S3, the Cu@MoS_2/PAAm/CA NCDN hydrogel catalyst is more consistent with Langmuir model because of a higher correlation coefficient (R^2 = 99.9%). This indicates that the adsorption of TC by the Cu@MoS_2/PAAm/CA NCDN hydrogel catalyst mainly conforms to the chemical adsorption of the Langmuir monolayer. To further study the adsorption mechanism of the Cu@MoS_2/PAAm/CA NCDN hydrogel catalyst, the kinetics was fitted to ascertain the rate-limiting process of TC adsorption. As revealed in Fig. S16 and Tab. S4–5, the adsorption process agrees with the pseudo-second-order kinetic model (R^2 = 99.9%), implying that chemical adsorption is the rate-determining step [28,50]. Detailed discussion is provided in the Supporting Information.

3.4. Degradation of TC

Adsorption can only transfer pollutants from wastewater to the adsorbent, but cannot degrade pollutants, making it difficult to regenerate the adsorbent. To address this issue, the photo-Fenton-like catalyst was integrated into the hydrogel to provide multiple abilities of adsorption, catalytic degradation, and degradation-driven self-regeneration. To show the advantages of the Cu@MoS_2/PAAm/CA NCDN hydrogel catalyst for efficient and rapid degradation of TC, a series of comparative experiments were carried out. Fig. 4a illustrates that the PAAm/SA hydrogel has no catalytic function in the degradation of TC, while the MoS_2/PAAm/SA hydrogel catalyst exhibits some degree of catalytic activity in the degradation of TC due to the Fenton-like interaction between MoS_2 and H_2O_2. The PAAm/CA hydrogel catalyst has considerable catalytic activity in the degradation of TC, because Cu^+/Cu^{2+} system can efficiently activate H_2O_2 to generate active species [16]. Thus, it is suggested that Cu^+/Cu^{2+} ions play a significant role in the Fenton-like degradation of TC. Notably, after adding MoS_2, the TC degradation efficiency of the Cu@MoS_2/PAAm/CA hydrogel catalyst increases remarkably and reaches 90% (degradation amount =

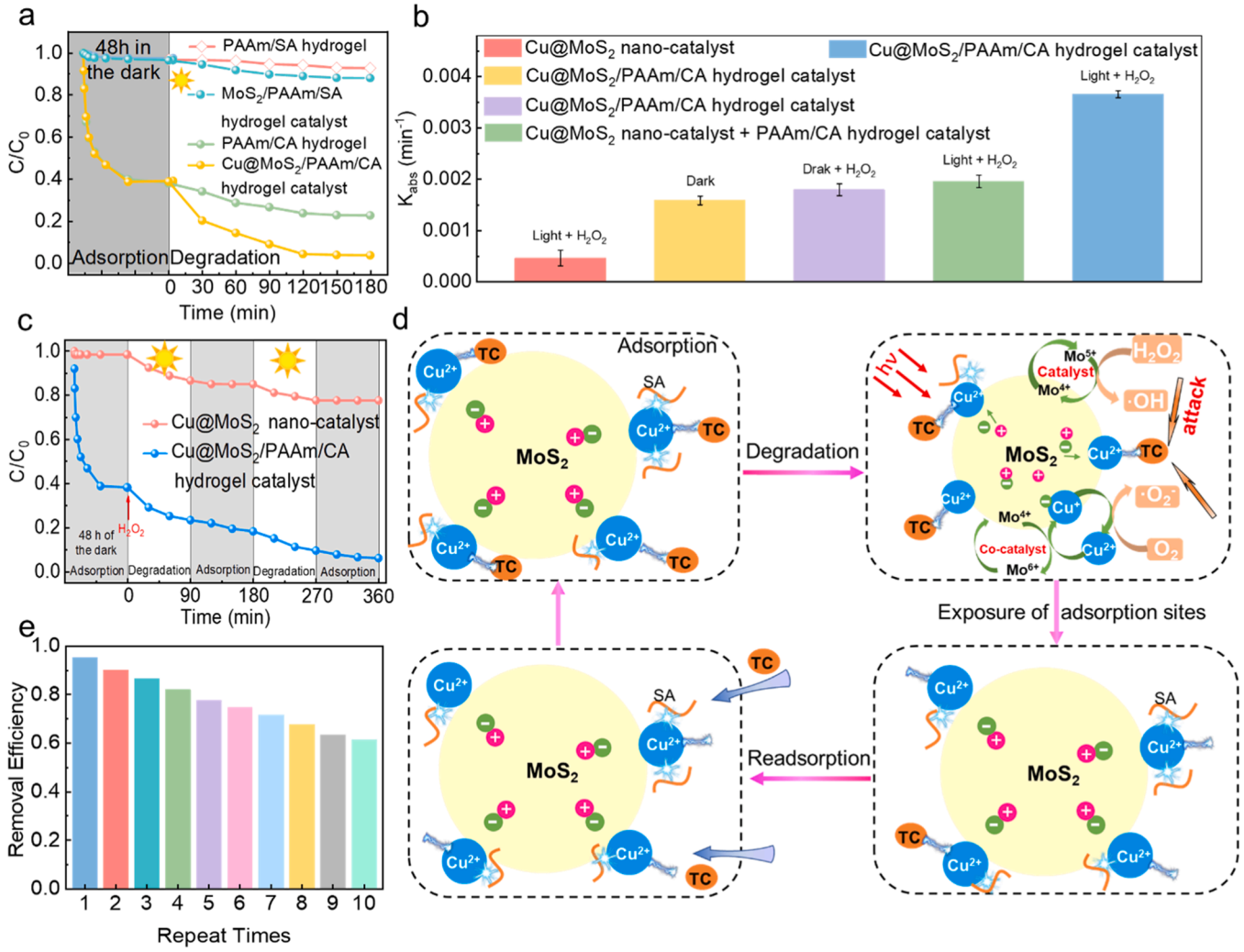

Fig. 4. (a) Performance of the PAAm/SA hydrogel, MoS_2/PAAm/CA hydrogel catalyst, PAAm/CA hydrogel catalyst, and Cu@MoS_2/PAAm/CA hydrogel catalyst in the adsorption and degradation of TC; (b) the reaction rate constants (k) of the TC degradation reactions in Fig. S19; (c) on-off light alternation experiments with the Cu@MoS_2 nano-catalyst and Cu@MoS_2/PAAm/CA hydrogel catalyst. The reaction conditions: 1.5 mmol L^{-1} H_2O_2 was only added once at 0 min; (d) possible mechanistic processes of the synergy of adsorption and catalytic degradation; (e) performance of the Cu@MoS_2/PAAm/CA hydrogel catalyst in pure adsorption and synergistic adsorption-catalytic degradation of TC during 10 reuse cycles.

70.2 mg g^{-1}) (Fig. 4a and Fig. S17). This is because MoS_2, as a Fenton-like catalyst and photocatalyst, has a synergistic effect with Cu ions, thereby boosting the generation of more active radical species and accelerating the degradation of TC [26]. Furthermore, the optimal H_2O_2 concentration for the degradation of TC by the Cu@MoS_2/PAAm/CA hydrogel catalysts was determined to be 1.5 mmol L^{-1} (Fig. S18).

In order to analyze the mutual promotion effect between adsorption and catalytic degradation, a series of comparative experiments were performed. As shown in Fig. S19 and Fig. 4b, the TC removal efficiency of the Cu@MoS_2/PAAM/CA hydrogel catalyst is 52.8% (removal amount = 105.6 mg g^{-1}) in the presence of H_2O_2 without light irradiation (Fig. 4b, Purple column). Furthermore, under light irradiation for 360 min, the TC removal efficiency is up to 76% (removal amount = 152.4 mg g^{-1}) (Fig. 4b, Blue column), which is 8 times higher than that of Cu@MoS_2 nano-catalyst (Fig. 4b, Red column). This is because the Cu@MoS_2/PAAM/CA hydrogel catalyst can adsorb a larger amount of TC, so that the active species can quickly capture and degrade TC. Specially, the TC removal efficiency is 46.3% (adsorption capacity = 92.6 mg g^{-1}) by mere adsorption of the Cu@MoS_2/PAAm/CA hydrogel catalyst in the dark without H_2O_2 (Fig. 4b, Yellow column). Compared with the single adsorption in the absence of H_2O_2 and light irradiation, the Cu@MoS_2/PAAm/CA hydrogel catalyst can eliminate TC on the adsorption sites through catalytic degradation in the presence of H_2O_2 and light irradiation, and the re-exposed adsorption sites can continue to adsorb TC from the solution, achieving the efficient cyclic adsorption-degradation (self-regeneration)-adsorption-degradation (self-regeneration) processes. Above phenomena indicate that the synergetic adsorption-catalytic degradation process is far superior to the single adsorption or single catalytic degradation process.

The advantages of the synergistic adsorption and catalytic degradation properties of the Cu@MoS_2/PAAm/CA hydrogel catalyst were further confirmed by comparison with the physical mixture of PAAm/CA hydrogel and Cu@MoS_2 nano-catalyst. When a physical mixture of 25 mg PAAm/CA hydrogel and 25 mg Cu@MoS_2 nano-catalyst was introduced to the TC solution, the removal efficiency of TC was 59% (degradation amount = 118.4 mg g^{-1}) (Fig. 4b, Green column), which was 17% lower than that of the Cu@MoS_2/PAAm/CA NCDN hydrogel catalyst. The physical mixture of PAAm/CA hydrogel and Cu@MoS_2 nano-catalyst failed to significantly improve the removal rate constant (k) of TC. The only difference of the physical mixture of PAAm/CA hydrogel and Cu@MoS_2 nano-catalyst from the Cu@MoS_2/PAAm/CA hydrogel catalyst is the separation of adsorption and catalytic degradation. Therefore, more enrichment of pollutants onto the catalyst and degradation-induced regeneration of the hydrogel adsorbent cannot be realized, resulting in very limited improvement in the TC removal performance of the physical mixture of PAAm/CA hydrogel and Cu@MoS_2 nano-catalyst.

To verify the self-regeneration ability of the Cu@MoS_2/PAAm/CA hydrogel catalyst, alternate on-off light experiments with the Cu@MoS_2 nano-catalyst and Cu@MoS_2/PAAm/CA hydrogel catalyst were performed. As indicated by Fig. 4c, the Cu@MoS_2 nano-catalyst had no apparent adsorption of TC after twice turning off the light. In contrast, the Cu@MoS_2/PAAm/CA hydrogel catalyst achieved 7.8 mg g^{-1} TC removal amount in the second dark stage. The Cu@MoS_2/PAAm/CA hydrogel catalyst can eliminate TC in both light and dark conditions, because the TC on the adsorption site is eliminated by catalytic degradation in light condition, resulting in self-regeneration of the hydrogel catalyst, and the re-exposure of the adsorption sites accompanying the degradation of TC in light condition enabled further adsorption of TC from the solution in dark condition. This phenomenon also shows the superiority of the synergistic effect between adsorption and catalytic degradation from another perspective.

The possible mechanistic processes of the synergy of adsorption and catalytic degradation are shown in Fig. 4d. The Cu@MoS_2/PAAm/CA NCDN hydrogel catalyst enriches a larger amount of TC around the bimetallic Fenton-like catalyst (Cu@MoS_2) by adsorption. The adsorption process shortens the distance between TC and the active species (such as •OH and $O_2^{\bullet-}$), and effectively improves the utilization rate of the active species. In addition to the active species produced through the Fenton-like processes (Eqs. (1−7)), the photogenerated electrons (e^-) and holes (h^+) can also be generated by MoS_2 during the irradiation process. The e^- are consumed in the reduction of Cu^{2+} to Cu^+ ($e^- + Cu^{2+} \rightarrow Cu^+$) [39], whereas the h^+ can react with H_2O_2 to produce $O_2^{\bullet-}$ ($h^+ + H_2O_2 \rightarrow O_2^{\bullet-} + 2\,H^+$) [51,52].

To evaluate the reusability of the Cu@MoS_2/PAAm/CA NCDN hydrogel catalyst, it was tested in the repeated TC removal experiments under the same conditions. Fig. 4e presents the results of TC removal during 10 consecutive reuse cycles of the Cu@MoS_2/PAAm/CA NCDN hydrogel catalyst. It can be seen from Fig. 4e that the removal of TC is 95% (removal amount = 190.5 mg g^{-1}) in the first cycle, while the removal of TC in the tenth cycle remains only 62% (removal amount = 122.1 mg g^{-1}). The Cu@MoS_2/PAAm/CA NCDN hydrogel catalyst was not lost during the recycling process, so the drop in its TC removal performance in the reuse cycles may be ascribed to the blockage of its pore structure and active sites by TC [31]. In addition, according to the ion leaching experiment (Fig. S20), the Cu ion leaching concentration after 15-day immersion was 0.91 mg L^{-1}, resulting in the reduction of the active sites, thus reducing the adsorption and degradation capacities.

3.5. Applicability

The influence of TC concentration on the TC removal efficiency by the Cu@MoS_2/PAAm/CA NCDN hydrogel catalyst is presented in Fig. 5a. With the increase of the initial TC concentration, the adsorption percentage decreased while the degradation percentage increased. Notably, the total TC removal percentage reached 96% for an initial TC concentration of 200 mg L^{-1}. This is due to the greatly enhanced TC adsorption capacity of the Cu@MoS_2/PAAm/CA NCDN hydrogel catalyst, facilitating the rapid reactions between active species and TC.

The impacts of interference factors, such as initial pH value, coexisting anions and other pollutants, and natural water quality, on the removal of TC by the Cu@MoS_2/PAAm/CA NCDN hydrogel catalyst were further researched, and the obtained results are as follows.

As Fig. 5b shows, the influence of initial pH value on the TC degradation was complex. The TC degradation amount first increased and then decreased as initial pH value increased from 3.0 to 7.0. The maximum TC degradation efficiency of 90% (degradation amount = 70.1 mg g^{-1}) was obtained at pH = 5.0, consistent with the influence of pH value on the adsorption of TC (Fig. 3c and S13).

As Fig. 5c shows, the anions (NO_3^-, HCO_3^-, HPO_4^{2-}, and Cl^-) not only impaired the TC adsorption performance of the Cu@MoS_2/PAAm/CA NCDN hydrogel catalyst, but also decreased its catalytic TC degradation performance. This may be due to the competitive adsorption and quenching of the active species (·OH) caused by these anions. The •OH radicals can be quenched by these anions through the reactions in Eqs. 8–11, and the oxidative activities of $NO_3^{\bullet}$, CO_3^{2-}, PO_4^{2-} and •ClOH are lower than •OH [18].

$$\cdot OH + NO_3^- \rightarrow OH^- + NO_3^{\bullet} \quad (8)$$

$$\cdot OH + HCO_3^- \rightarrow CO_3^{2-} + H_2O \quad (9)$$

$$\cdot OH + HPO_4^{2-} \rightarrow PO_4^{3-} + H_2O \quad (10)$$

$$\cdot OH + Cl^- \rightarrow \cdot ClOH \quad (11)$$

As Fig. 5d shows, the Cu@MoS_2/PAAm/CA NCDN hydrogel catalyst exhibited also outstanding performance in the adsorption and catalytic degradation of methylene blue (MB), sulfamethoxazole (SMX), levofloxacin (LFX) and ciprofloxacin (CIP), with the removal efficiencies of MB, SMX, LFX and CIP being as high as 97%, 73%, 79%, 83%, respectively, proving its versatility.

As Fig. 5e shows, the removal rates of TC in tap water and lake water

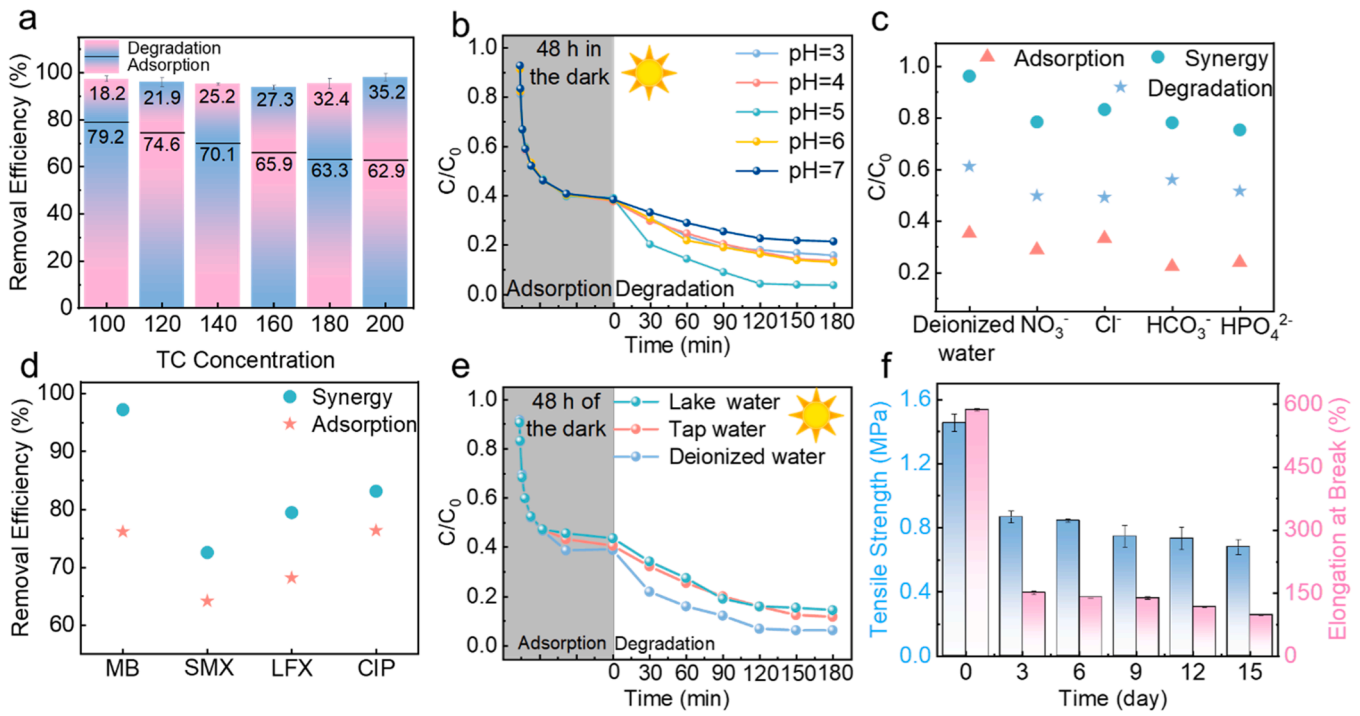

Fig. 5. Impacts of (a) initial TC concentration, (b) initial pH value, and (c) coexisting anions on the TC removal by the Cu@MoS_2/PAAm/CA NCDN hydrogel catalyst; (d) removal of various organic pollutants by the Cu@MoS_2/PAAm/CA NCDN hydrogel catalyst; (e) influence of real water bodies on the TC removal by the Cu@MoS_2/PAAm/CA NCDN hydrogel catalyst; (f) the subaqueous mechanical properties of the Cu@MoS_2/PAAm/CA NCDN hydrogel catalyst over 5 cycles. The reaction conditions: [hydrogel catalyst] = 50 mg, [H_2O_2] = 1.5 mmol L^{-1}, [TC] = 200 mg L^{-1}, [methylene blue MB] = [sulfamethoxazole SMX] = [levofloxacin LFX] = [ciprofloxacin CIP] = 40 mg L^{-1}, [NO^{3-}] = [Cl^-] = [HCO_3] = [HPO_4^{2-}] = 5 mmol L^{-1}.

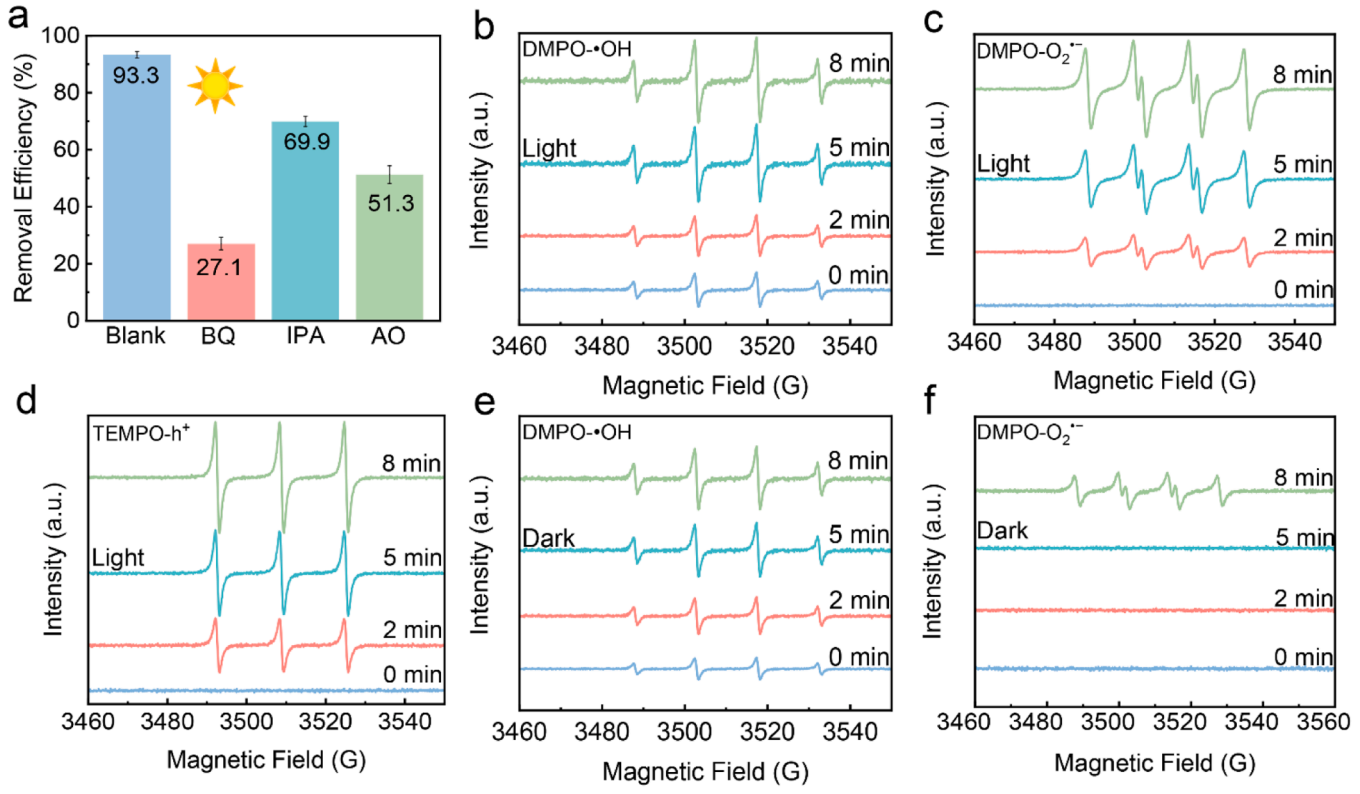

Fig. 6. (a) Results from the active species trapping experiments for TC degradation by the Cu@MoS_2/PAAm/CA NCDN hydrogel catalyst in photo-Fenton-like reaction; EPR spectra of (b) DMPO-·OH, (c) DMPO-$O_2^{\bullet-}$ and (d) TEMPO-h^+ detected in the Cu@MoS_2/PAAm/CA + H_2O_2 + light reaction system at different irradiation times; (e) DMPO-·OH and (f) DMPO-$O_2^{\bullet-}$ detected in the Cu@MoS_2/PAAm/CA + H_2O_2 + dark reaction system at different times. The reaction conditions: [hydrogel catalyst] = 50 mg, [H_2O_2] = 1.5 mmol L^{-1}, [TC] = 200 mg L^{-1}, [BQ] = [IPA] = [AO] = 0.1 mol L^{-1}.

decreased slightly in comparison with that in deionized water, due to the presence of more organic compounds and inorganic ions [24,52]. Nevertheless, the Cu@MoS_2/PAAm/CA NCDN hydrogel catalyst still had fairly high efficiencies in eliminating TC in tap water and lake water. Thus, the Cu@MoS_2/PAAm/CA NCDN hydrogel catalyst possesses promising application prospects in practical wastewater treatment.

The mechanical durability of the Cu@MoS_2/PAAm/CA NCDN hydrogel catalyst is also a crucial aspect affecting its application in wastewater treatment. As Fig. 5f shows, even after a 15-day immersion in water, the tensile strength of the Cu@MoS_2/PAAm/CA NCDN hydrogel catalyst remained high at 0.68 MPa. This performance surpasses those of most unsoaked hydrogel products, demonstrating a long-term subaqueous stability. These results strongly prove that the Cu@MoS_2/PAAm/CA hydrogel catalyst has remarkable reusability, stability and recyclability in aqueous environment.

3.6. The synergistic mechanism

The Cu@MoS_2/PAAm/CA hydrogel catalyst displays excellent performance in the degradation of TC through photo-Fenton-like reaction. To identify the major active species in the degradation of TC by the Cu@MoS_2/PAAm/CA hydrogel catalyst, the active species trapping experiments were conducted. Benzoquinone (BQ), ammonium oxalate (AO), and isopropanol (IPA) were utilized in turn as the scavenging agents for superoxide radicals ($O_2^{\bullet-}$), photogenerated holes (h^+), and hydroxyl radicals (·OH). As can be seen from Fig. 6a and S21, different scavengers show diverse inhibitory effects on the TC degradation. The addition of BQ significantly inhibits the TC degradation. The addition of 0.05 mol L^{-1} and 0.1 mol L^{-1} BQ leads to decreases in TC removal from 93.3% (degradation amount = 72.2 mg g^{-1}) to 37.9% (degradation amount = 29.3 mg g^{-1}) and 27.1% (degradation amount =21.0 mg g^{-1}), respectively, showing that $O_2^{\bullet-}$ is the dominant species involved in the TC degradation reactions. Moreover, AO and IPA also exhibit inhibitory effects on the degradation of TC. The TC degradation efficiency gradually decreases as the dosages of AO and IPA increase from 0.05 to 0.2 mol L^{-1}, demonstrating that h^+ and·OH radicals also participate in the TC degradation reactions, and the role of h^+ ranks only second to $O_2^{\bullet-}$.

In the dark-Fenton-like reaction, after the addition of BQ (0.1 mol L^{-1}) and IPA (0.1 mol L^{-1}) to the solution, the TC removal rate decreases from 72.7% (degradation amount = 56.3 mg g^{-1}) to 58.1% (degradation amount = 44.9 mg g^{-1}) and 33.2% (degradation amount = 25.7 mg g^{-1}), respectively (Fig. S22). These results show that·OH is the major active species for the dark-Fenton-like reaction, followed by $O_2^{\bullet-}$. This is because that the amount of $O_2^{\bullet-}$ produced under dark conditions is reduced (in the darkness, photogenerated holes and electrons cannot be generated by the Cu@MoS_2/PAAm/CA hydrogel catalyst, and thus $O_2^{\bullet-}$ cannot be generated through the pathway of $h^+ + H_2O_2 \rightarrow O_2^{\bullet-} + 2\,H^+$, $O_2 + e^- \rightarrow O_2^{\bullet-}$).

Further EPR results are consistent with active species trapping experiment results. The generations of·OH, $O_2^{\bullet-}$ and h^+ by the Cu@MoS_2/PAAm/CA hydrogel catalyst in TC degradation were investigated via EPR test (Fig. 6b-f). The DMPO-·OH (1:2:2:1), DMPO-$O_2^{\bullet-}$ (1:1:1:1) and DMPO- h^+ (1:1:1) signals can be detected in the reaction system of Cu@MoS_2/PAAm/CA + H_2O_2 + light irradiation, and their intensities progressively increase with irradiation time (Fig. 6b-d). For the dark-Fenton-like system, the EPR signals of both DMPO-·OH (1:2:2:1) and DMPO-$O_2^{\bullet-}$ (1:1:1:1) are also detected, but their intensities are weaker than those in photo-Fenton-like reaction (Fig. 6e, f). Thus, $O_2^{\bullet-}$ is the main active species, h^+ and·OH are the minor active species in the photo-Fenton-like system, while·OH is the primary active species and $O_2^{\bullet-}$ is the secondary active species in the dark-Fenton-like system.

To further study the removal mechanism, the XPS spectra of the Cu@MoS_2/PAAm/CA hydrogel catalyst were examined before and after TC degradation, as shown in Fig. 7a-b and S23. It is evident that the peak positions of the main elements in the Cu@MoS_2/PAAm/CA hydrogel catalyst keep essentially unchanged before and after the reaction.

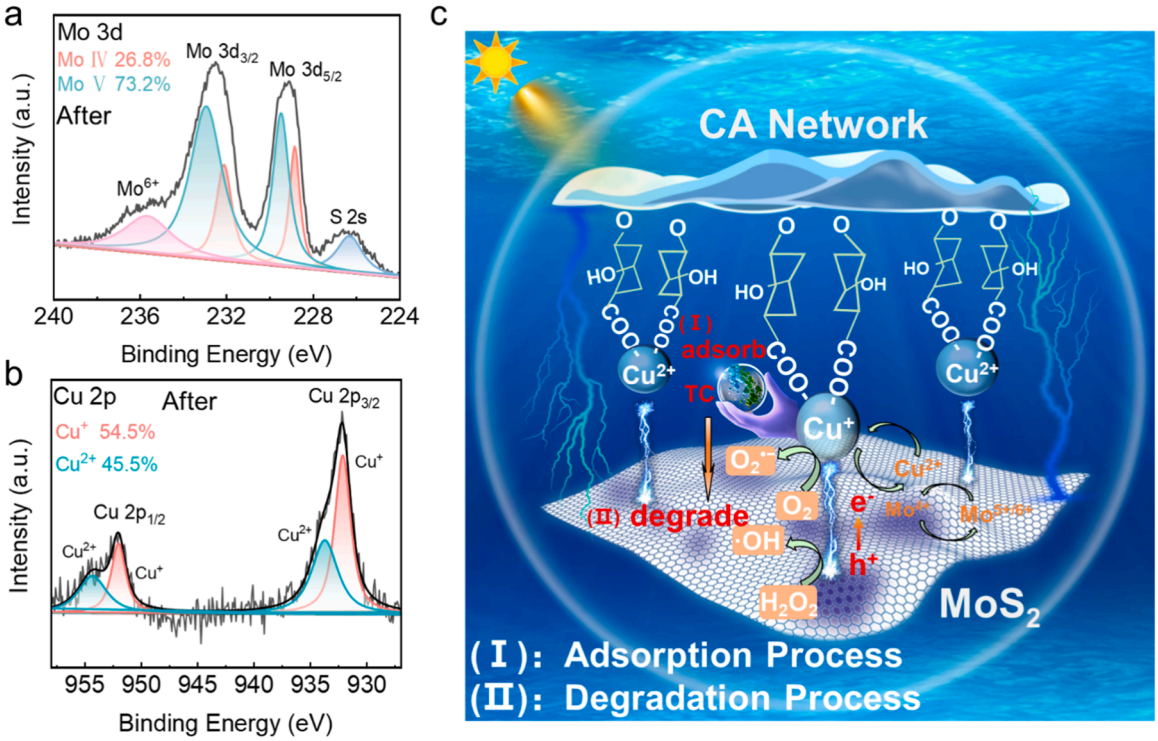

Fig. 7. XPS spectra of the Cu@MoS_2/PAAm/CA hydrogel catalyst after catalytic degradation of TC: (a) Mo 3d, (b) Cu 2p. (c) Mechanism of the adsorption and catalytic degradation of TC by the Cu@MoS_2/PAAm/CA NCDN hydrogel catalyst. The reaction conditions: [TC] = 200 mg L^{-1}, [catalyst] = 50 mg, [H_2O_2] = 5.0 mmol L^{-1}.

However, XPS elemental peak area analysis certifies changes in the chemical valence, Mo^{4+}/Mo^{5+} and Cu^{2+}/Cu^{+} ratios following the degradation reaction. As shown in Fig. 7 and S23, the content of Mo^{4+} diminishes while those of Mo^{5+} and Mo^{6+} improve after the TC degradation. The Cu content analysis reveals an increase in Cu^{+} from 44.8% to 54.5% and a decrease in Cu^{2+} from 55.2% to 45.5% after catalytic degradation of TC, suggesting the transformation between Cu^{2+} and Cu^{+} (Eqs. 1–7).

In addition, the possible degradation products were identified through the HPLC-MS analysis (Fig. S24), and four degradation routes as shown in Fig. S25 were presumed. The details of the four degradation routes are described in Supporting Information. As illustrated in Fig. S26, the total organic carbon (TOC) of TC solution decreases from 277 to 94.2 mg L^{-1} (66% TOC removal efficiency) when exposed to light irradiation for 180 min

Based on the above results, the synergistic effect between adsorption and catalytic degradation functions of the Cu@MoS_2/PAAm/CA hydrogel catalyst can achieve mutual promotion, which is more efficient than single adsorption or single catalytic degradation process. The adsorption process can enrich TC onto the bimetallic Fenton-like catalyst, facilitating the reactions of TC with the active species [21]. According to the adsorption mechanism, $(-COO)_2Cu$ plays a "bridge" role in the TC adsorption based on the Hard-Soft-Acid-Base theory and the spatial effect. As shown in Fig. 7c (I), the high-capacity adsorption captures TC around the bimetallic Fenton-like Cu@MoS_2 catalyst. This reduces the travel distance of the reactive species and accelerates the reaction rate. Then, as depicted in Fig. 7c (II), the bimetallic photo-Fenton-like catalyst can generate various free radicals in the presence of H_2O_2 and light irradiation to degrade TC, realizing the regeneration of adsorption sites and enabling the efficient cyclic adsorption-degradation (self-regeneration)-adsorption-degradation (self-regeneration) processes. Thus, the synergy of adsorption and catalytic degradation can be a valuable way to eliminate pollutants.

4. Conclusions

A novel Cu@MoS_2/PAAm/CA NCDN hydrogel catalyst was prepared and applied to treat high concentration TC in water. The Cu@MoS_2/PAAm/CA NCDN hydrogel catalyst displayed outstanding adsorption capacity, which can enrich TC around the Cu@MoS_2 photo-Fenton-like catalyst and greatly improve the degradation efficiency of TC. Meanwhile, the catalytic degradation process degraded TC and regenerated the adsorption sites. Consequently, efficient removal of TC has been realized in both light and dark environment. This study proves that the synergy of adsorption and catalytic degradation is a very effective strategy to eliminate TC from water.

Another notable achievement of this study is the demonstration of the practical value of hydrogel as a supporting material for nano-catalyst. The Cu@MoS_2/PAAm/CA NCDN hydrogel catalyst exhibited several advantages. Firstly, it has high adsorption capacity for TC due to its 3D porous structure, large surface area, and outstanding hydrophilicity. Secondly, Cu/MoS_2 nano-catalyst is uniformly immobilized on the hydrogel, which not only solves the problem of recycling, but also enables more contact between Cu@MoS_2 and pollutants. Furthermore, the coordination effect of the CA network and MoS_2 provides spatial constraints that shorten the distance between the catalyst surface and the reactants, improving the utilization efficiency of the active radicals. Finally, the Cu@MoS_2/PAAm/CA NCDN hydrogel catalyst possesses remarkable mechanical properties, which endow the catalyst with outstanding durability and recyclability. Therefore, the Cu@MoS_2/PAAm/CA NCDN hydrogel catalyst with great synergistic effect between adsorption and catalytic degradation, good recyclability, excellent mechanical performance, and outstanding durability can be expected to have practical application prospect for the elimination of antibiotics and other contaminants of emerging concern in water.

CRediT authorship contribution statement

Song Xiaoyu: Investigation, Methodology, Writing – original draft. **Qin Gang:** Conceptualization, Project administration, Resources, Writing – original draft. **Zhang Yongcai:** Supervision, Writing – review & editing. **Dionysiou Dionysios D.:** Writing – review & editing. **Li Yue:** Funding acquisition, Supervision, Writing – review & editing. **Yang Jia:** Methodology. **He Wenjie:** Data curation. **Chen Qiang:** Investigation.

Declaration of Competing Interest

We declare that we have no known competing financial interests or personal relationships that could have appeared to influence the work reported in this paper.

Data Availability

Data will be made available on request.

Acknowledgements

This work was financially supported by the National Natural Science Foundation of China (No. 52370073), Natural Science Foundation of Henan Province (212300410336), Program for Science and Technology Innovation Team in Universities of Henan Province (24IRTSTHN017), Major Project of WIUCAS (WIUCASQD2021004 and WIUCASQD2021035), Key Scientific and Technological Project of Henan Province (222102320188), Key Project of Science and Technology Research of Henan Provincial Department of Education (21A430008), The project of national local joint engineering laboratory to functional adsorption material technology for the environmental protection, Soochow University (SDGC2124).

Appendix A. Supporting information

Supplementary data associated with this article can be found in the online version at doi:10.1016/j.apcatb.2023.123640.

References

[1] C.-Y. Wang, X. Zhang, H.-B. Qiu, G.-X. Huang, H.-Q. Yu, $Bi_{24}O_{31}Br_{10}$ nanosheets with controllable thickness for visible–light–driven catalytic degradation of tetracycline hydrochloride, Appl. Catal. B: Environ. 205 (2017) 615–623.
[2] X.-H. Yi, T.-Y. Wang, H.-Y. Chu, Y. Gao, C.-C. Wang, Y.-J. Li, L. Chen, P. Wang, H. Fu, C. Zhao, W. Liu, Effective elimination of tetracycline antibiotics via photoactivated SR-AOP over vivianite: A new application approach of phosphorus recovery product from WWTP, Chem. Eng. J. 449 (2022), 137784.
[3] Y. Li, B. Yu, H. Li, B. Liu, X. Yu, K. Zhang, G. Qin, J. Lu, L. Zhang, L. Wang, Activation of hydrogen peroxide by molybdenum disulfide as Fenton-like catalyst and cocatalyst: Phase-dependent catalytic performance and degradation mechanism, Chin. Chem. Lett. 34 (2023), 107874.
[4] K.S.D. Premarathna, A.U. Rajapaksha, N. Adassoriya, B. Sarkar, N.M.S. Sirimuthu, A. Cooray, Y.S. Ok, M. Vithanage, Clay-biochar composites for sorptive removal of tetracycline antibiotic in aqueous media, J. Environ. Manag. 238 (2019) 315–322.
[5] Y. Wang, Z. Qiang, W. Zhu, W. Yao, S. Tang, Z. Yang, J. Wang, J. Duan, C. Ma, R. Tan, $BiPO_4$ Nanorod/Graphene Composite Heterojunctions for Photocatalytic Degradation of Tetracycline Hydrochloride, ACS Appl. Nano Mater. 4 (2021) 8680–8689.
[6] J. Xue, D. Lei, X. Zhao, Y. Hu, S. Yao, K. Lin, Z. Wang, C. Cui, Antibiotic residue and toxicity assessment of wastewater during the pharmaceutical production processes, Chemosphere 291 (2022), 132837.
[7] C. Xia, H. Huang, D. Liang, Y. Xie, F. Kong, Q. Yang, J. Fu, Z. Dou, Q. Zhang, Z. Meng, Adsorption of tetracycline hydrochloride on layered double hydroxide loaded carbon nanotubes and site energy distribution analysis, Chem. Eng. J. 443 (2022), 136398.
[8] L. Du, S. Ahmad, L. Liu, L. Wang, J. Tang, A review of antibiotics and antibiotic resistance genes (ARGs) adsorption by biochar and modified biochar in water, Sci. Total Environ. 858 (2023), 159815.
[9] R. Geng, J. Wang, Z. Zhang, Q. Dong, F. Wu, S. Chen, T. Su, X. Qi, Adsorption of antibiotics by polydopamine-modified salecan hydrogel: Performance, kinetics and mechanism studies, Chem. Eng. J. 454 (2023), 140446.
[10] H. Peng, W. Xiong, Z. Yang, J. Cao, M. Jia, Y. Xiang, Q. Hu, Z. Xu, Facile fabrication of three-dimensional hierarchical porous ZIF-L/gelatin aerogel: Highly efficient

adsorbent with excellent recyclability towards antibiotics, Chem. Eng. J. 426 (2021), 130798.
[11] W. Gao, Y. Chen, B. Li, S.P. Liu, X. Liu, Q. Jiang, Determining the adsorption energies of small molecules with the intrinsic properties of adsorbates and substrates, Nature, Communications 11 (2020) 1196.
[12] W. Wang, Y. Cao, X. Hu, S. Zhou, D. Zhu, D. Qi, S. Deng, Granular reduced graphene oxide/Fe_3O_4 hydrogel for efficient adsorption and catalytic oxidation of p-perfluorous nonenoxybenzene sulfonate, J. Hazard. Mater. 386 (2020), 121662.
[13] Q. Wu, M.S. Siddique, Y. Guo, M. Wu, Y. Yang, H. Yang, Low-crystalline bimetallic metal-organic frameworks as an excellent platform for photo-Fenton degradation of organic contaminants: Intensified synergism between hetero-metal nodes, Appl. Catal. B: Environ. 286 (2021), 119950.
[14] Z. Wang, F. Bai, L. Cao, S. Yue, J. Wang, S. Wang, J. Ma, P. Xie, Activation of sulfite by ferric ion for the degradation of 2,4,6-tribromophenol with the addition of sulfite in batches, Chin. Chem. Lett. 33 (2022) 4766–4770.
[15] X.-W. Zhang, M.-Y. Lan, F. Wang, C.-C. Wang, P. Wang, C. Ge, W. Liu, Immobilized N-C/Co derived from ZIF-67 as PS-AOP catalyst for effective tetracycline matrix elimination: From batch to continuous process, Chem. Eng. J. 450 (2022), 138082.
[16] D.A. Nichela, A.M. Berkovic, M.R. Costante, M.P. Juliarena, F.S. García Einschlag, Nitrobenzene degradation in Fenton-like systems using Cu(II) as catalyst. Comparison between Cu(II)- and Fe(III)-based systems, Chem. Eng. J. 228 (2013) 1148–1157.
[17] C. Xu, Q. Zhou, W.-Y. Huang, K. Yang, Y.-C. Zhang, T.-X. Liang, Z.-Q. Liu, Constructing Z-scheme β-Bi2O_3/ZrO_2 heterojunctions with 3D mesoporous SiO_2 nanospheres for efficient antibiotic remediation via synergistic adsorption and photocatalysis, Rare Met. 41 (2022) 2094–2107.
[18] Q. Xia, D. Zhang, Z. Yao, Z. Jiang, Investigation of Cu heteroatoms and Cu clusters in Fe-Cu alloy and their special effect mechanisms on the Fenton-like catalytic activity and reusability, Appl. Catal. B: Environ. 299 (2021), 120662.
[19] Y. Wang, H. Song, J. Chen, S. Chai, L. Shi, C. Chen, Y. Wang, C. He, A novel solar photo-Fenton system with self-synthesizing H_2O_2: Enhanced photo-induced catalytic performances and mechanism insights, Appl. Surf. Sci. 512 (2020), 145650.
[20] L. Lyu, C. Lu, Y. Sun, W. Cao, T. Gao, C. Hu, Low consumption Fenton-like water purification through pollutants as electron donors substituting H_2O_2 consumption via twofold cation-π over MoS_2 cross-linking g-C_3N_4 hybrid, Appl. Catal. B: Environ. 320 (2023), 121871.
[21] Y. Ren, J. Yu, J. Zhang, L. Lv, W. Zhang, An in-situ strategy to analyze multi-effect catalysis in iron-copper bimetals catalyzed Fenton-like processes, Appl. Catal. B: Environ. 299 (2021), 120697.
[22] J. Li, H. Yuan, Z. Zhu, Improved photoelectrochemical performance of Z-scheme g-C_3N_4/Bi_2O_3/$BiPO_4$ heterostructure and degradation property, Appl. Surf. Sci. 385 (2016) 34–41.
[23] B. Khan, F. Raziq, M. Bilal Faheem, M. Umar Farooq, S. Hussain, F. Ali, A. Ullah, A. Mavlonov, Y. Zhao, Z. Liu, H. Tian, H. Shen, X. Zu, S. Li, H. Xiao, X. Xiang, L. Qiao, Electronic and nanostructure engineering of bifunctional MoS_2 towards exceptional visible-light photocatalytic CO_2 reduction and pollutant degradation, J. Hazard. Mater. 381 (2020), 120972.
[24] Y. Lv, P. Chen, J.J. Foo, J. Zhang, W. Qian, C. Chen, W.J. Ong, Dimensionality-dependent MoS_2 toward efficient photocatalytic hydrogen evolution: from synthesis to modifications in doping, surface and heterojunction engineering, Mater. Today Nano 18 (2022), 100191.
[25] H. Zhang, L. Deng, J. Chen, Y. Zhang, M. Liu, Y. Han, Y. Chen, H. Zeng, Z. Shi, How MoS_2 assisted sulfur vacancies featured Cu_2S in hollow Cu_2S@MoS_2 nanoboxes to activate H_2O_2 for efficient sulfadiazine degradation? Chem. Eng. J. 446 (2022), 137364.
[26] Y. Yang, W. Zhen, T. Zhao, M. Wu, S. Ma, L. Zhao, J. Wu, L. Liu, J. Zhang, T. Yao, Engineering low-valence $Mo^{\delta+}$ (0<δ<4) sites on MoS2 surface: Accelerating Fe3+/Fe2+ cycle, maximizing H2O2 activation efficiency, and extending applicable pH range in photo-Fenton reaction, J. Clean. Prod. 404 (2023), 136918.
[27] B. Yan, C. Ma, J. Gao, Y. Yuan, N. Wang, An ion-crosslinked supramolecular hydrogel for ultrahigh and fast uranium recovery from seawater, Adv. Mater. 32 (2020) 1906615.
[28] Z. Wu, P. Zhang, H. Zhang, X. Li, Y. He, P. Qin, C. Yang, Tough porous nanocomposite hydrogel for water treatment, J. Hazard. Mater. 421 (2022), 126754.
[29] F. Yu, P. Yang, Z. Yang, X. Zhang, J. Ma, Double-network hydrogel adsorbents for environmental applications, Chem. Eng. J. 426 (2021), 131900.
[30] D. Li, W. Zhan, W. Zuo, L. Li, J. Zhang, G. Cai, Y. Tian, Elastic, tough and switchable swelling hydrogels with high entanglements and low crosslinks for water remediation, Chem. Eng. J. 450 (2022), 138417.
[31] Q. Luo, T. Ren, Z. Lei, Y. Huang, Y. Huang, D. Xu, C. Wan, X. Guo, Y. Wu, Non-toxic chitosan-based hydrogel with strong adsorption and sensitive detection abilities for tetracycline, Chem. Eng. J. 427 (2022), 131738.
[32] S. Tang, J. Yang, L. Lin, K. Peng, Y. Chen, S. Jin, W. Yao, Construction of physically crosslinked chitosan/sodium alginate/calcium ion double-network hydrogel and its application to heavy metal ions removal, Chem. Eng. J. 393 (2020), 124728.
[33] C.H. Lu, Y.C. Yeh, Fabrication of multiresponsive magnetic nanocomposite double-network hydrogels for controlled release applications, Small 17 (2021) 2105997.
[34] A. Kumar, K.M. Rao, S.S. Han, Synthesis of mechanically stiff and bioactive hybrid hydrogels for bone tissue engineering applications, Chem. Eng. J. 317 (2017) 119–131.
[35] J. Zeng, L. Dong, W. Sha, L. Wei, X. Guo, Highly stretchable, compressible and arbitrarily deformable all-hydrogel soft supercapacitors, Chem. Eng. J. 383 (2020), 123098.
[36] J. Fan, Z. Shi, M. Lian, H. Li, J. Yin, Mechanically strong graphene oxide/sodium alginate/polyacrylamide nanocomposite hydrogel with improved dye adsorption capacity, J. Mater. Chem. A 1 (2013) 7433.
[37] L. Wang, G. Yu, J. Li, Y. Feng, Y. Peng, X. Zhao, Y. Tang, Q. Zhang, Stretchable hydrophobic modified alginate double-network nanocomposite hydrogels for sustained release of water-insoluble pesticides, J. Clean. Prod. 226 (2019) 122–132.
[38] X. Zhang, B. Lin, K. Zhao, J. Wei, J. Guo, W. Cui, S. Jiang, D. Liu, J. Li, A free-standing calcium alginate/polyacrylamide hydrogel nanofiltration membrane with high anti-fouling performance: Preparation and characterization, Desalination 365 (2015) 234–241.
[39] C. Wang, J. Li, X. Liu, Z. Cui, D.F. Chen, Z. Li, Y. Liang, S. Zhu, S. Wu, The rapid photoresponsive bacteria-killing of Cu-doped MoS_2, Biomater. Sci. 8 (2020) 4216–4224.
[40] O. Sreekanth Reddy, M.C.S. Subha, T. Jithendra, C. Madhavi, K. Chowdoji Rao, Curcumin encapsulated dual cross linked sodium alginate/montmorillonite polymeric composite beads for controlled drug delivery, J. Pharm. Anal. 11 (2021) 191–199.
[41] F. Sheng, J. Yi, S. Shen, R. Cheng, C. Ning, L. Ma, X. Peng, W. Deng, K. Dong, Z. L. Wang, Self-powered smart arm training band sensor based on extremely stretchable hydrogel conductors, ACS Appl. Mater. Interfaces 13 (2021) 44868–44877.
[42] D. Zhao, M. Feng, L. Zhang, B. He, X. Chen, J. Sun, Facile synthesis of self-healing and layered sodium alginate/polyacrylamide hydrogel promoted by dynamic hydrogen bond, Carbohydr. Polym. 256 (2021), 117580.
[43] H. Yang, H. Lu, Y. Miao, Y. Cong, Y. Ke, J. Wang, H. Yang, J. Fu, Non-swelling, super-tough, self-healing, and multi-responsive hydrogels based on micellar crosslinking for smart switch and shape memory, Chem. Eng. J. 450 (2022), 138346.
[44] Z. Yang, S. Jia, T. Zhang, N. Zhuo, Y. Dong, W. Yang, Y. Wang, How heavy metals impact on flocculation of combined pollution of heavy metals–antibiotics: A comparative study, Sep. Purif. Technol. 149 (2015) 398–406.
[45] M.H. Khan, H. Bae, J.Y. Jung, Tetracycline degradation by ozonation in the aqueous phase: proposed degradation intermediates and pathway, J. Hazard. Mater. 181 (2010) 659–665.
[46] Z. Zhang, Y. Chen, Z. Wang, C. Hu, D. Ma, W. Chen, T. Ao, Effective and structure-controlled adsorption of tetracycline hydrochloride from aqueous solution by using Fe-based metal-organic frameworks, Appl. Surf. Sci. 542 (2021), 148662.
[47] H. Qian, Y.-L. Lin, B. Xu, L.-P. Wang, Z.-C. Gao, N.-Y. Gao, Adsorption of haloforms onto GACs: Effects of adsorbent properties and adsorption mechanisms, Chem. Eng. J. 349 (2018) 849–859.
[48] S. Zhang, Y. Dong, Z. Yang, W. Yang, J. Wu, C. Dong, Adsorption of pharmaceuticals on chitosan-based magnetic composite particles with core-brush topology, Chem. Eng. J. 304 (2016) 325–334.
[49] W. Xiang, Y. Wan, X. Zhang, Z. Tan, T. Xia, Y. Zheng, B. Gao, Adsorption of tetracycline hydrochloride onto ball-milled biochar: Governing factors and mechanisms, Chemosphere 255 (2020), 127057.
[50] C. Mu, Y. Zhang, W. Cui, Y. Liang, Y. Zhu, Removal of bisphenol A over a separation free 3D Ag_3PO_4-graphene hydrogel via an adsorption-photocatalysis synergy, Appl. Catal. B: Environ. 212 (2017) 41–49.
[51] H. Xu, X. Liu, H. Li, L. Zhang, O_2 activation and $^1O_2$ generation over phosphate modified BiOCl for efficient photodegradation of organic pollutants, Appl. Catal. B: Environ. 314 (2022), 121520.
[52] Y. Li, B. Yu, B. Liu, X. Yu, G. Qin, M. Fan, Y. Zhang, L. Wang, Superior Fenton-like and photo-Fenton-like activity of MoS_2@TiO_2/N-doped carbon nanofibers with phase-regulated and vertically grown MoS2 nanosheets, Chem. Eng. J. 452 (2023), 139542.